

## Discrete-ordinate method of solution of Fokker-Planck equations with nonlinear coefficients

R. Blackmore and B. Shizgal

*Department of Chemistry, University of British Columbia, Vancouver, British Columbia, Canada V6T 1Y6*

(Received 3 July 1984)

A discrete-ordinate method [J. Comput. Phys. 55, 313 (1984)] based on nonclassical polynomials is applied to the solution of a large class of Fokker-Planck equations with nonlinear coefficients. These Fokker-Planck equations arise in the description of nonequilibrium processes in reactive systems, laser systems, and model systems with bistable potentials. This subject has received considerable attention in recent years in connection with stochastic processes in physics, cooperative phenomena, and synergetics. The present approach is based on an eigenfunction expansion of the time-dependent probability density function. A discrete-ordinate method is employed in a numerical calculation of the eigenvalues and corresponding eigenfunctions of the Fokker-Planck operator. A general procedure for determining the eigenvalue spectrum of such Fokker-Planck operators with the discrete-ordinate method based on nonclassical polynomials, constructed so as to give rapid convergence of the eigenvalues, is described. The method is applied to several systems which include a model problem for which an analytic solution is known, a model with a triple-well potential in the Schrödinger equation equivalent to the Fokker-Planck equation, and to a model for the *trans-gauche* isomerization of *n*-butane in carbon tetrachloride. The present methods for studying eigenvalue and boundary-value problems should be applicable to a wide variety of problems in addition to those presented here.

### I. INTRODUCTION

The Fokker-Planck equation (FPE) with nonlinear drift and diffusion terms is often employed to describe the time evolution of nonequilibrium systems in physics, chemistry, biology, and the applied sciences.<sup>1-3</sup> Some of the physical problems considered include model systems for Brownian motion and diffusion,<sup>4-9</sup> chemically reactive systems,<sup>10-14</sup> laser systems,<sup>15-19</sup> and many other applications. Much of the attention devoted to such problems in recent years is due to the relationship of such models to the study of nonequilibrium phenomena, cooperative phenomena, and synergetics.<sup>1-3</sup>

A study based on the (one-dimensional) FPE concerns itself with the probability density function (PDF)  $P(x,t)$ , which gives the probability that a macroscopic property will take on a specific value  $x$  at time  $t$ . The purpose of the present paper is to apply a recently developed discrete-ordinate method to the solution of the FPE of the form

$$\frac{\partial P(x,t)}{\partial t} = \frac{\partial[A(x)P(x,t)]}{\partial x} + \frac{\partial^2[B(x)P(x,t)]}{\partial x^2}, \quad (1)$$

where  $A(x)$  and  $B(x)$  are generally referred to as the drift and diffusion coefficients, respectively. The explicit forms of  $A(x)$  and  $B(x)$  vary considerably and depend on the particular application considered.<sup>2</sup> It is useful to note that Eq. (1) is a linear differential equation with coefficients  $A(x)$  and  $B(x)$  which may be linear or nonlinear functions of  $x$ .

For certain choices of these coefficients, there are special solutions worthy of mention. For example, with

$A(x) = x^{-3/2}$  and  $B(x) = x$ , the FPE is an approximation to the Boltzmann equation of kinetic theory for the relaxation of an ensemble of infinitely heavy particles dilutely dispersed in a heat bath of light particles (the Rayleigh problem), interacting via hard-sphere collisions.<sup>20,21</sup> The equilibrium state is a Maxwellian (Gaussian) distribution, and the PDF  $P(x,t)$  is known analytically for an initial  $\delta$  function distribution and for an initial Gaussian distribution. For an initial Gaussian distribution,  $P(x,t)$  remains Gaussian with a time-dependent variance or temperature.

For the analogous relaxation of infinitely light particles in a heat bath of heavy particles (the Lorentz problem),  $A(x) = (x-2)x^{1/2}$  and  $B(x) = x^{3/2}$ .<sup>20,21</sup> In this case, a simple analytic solution comparable to the Rayleigh problem is not known. This situation has the physically important application to the study of the thermalization of electrons in gaseous systems, which has been discussed elsewhere.<sup>22,23</sup> A variety of special soluble Fokker-Planck equations have been discussed by other authors.<sup>24-27</sup>

The present work focuses on problems for which  $A(x)$  and  $B(x)$  are nonlinear such that the equilibrium solution may possess two states; that is,  $P(x, \infty)$  is bimodal. For such systems, there is the possibility for the time-dependent solution to exhibit a bifurcation and the solution will in general depend on the initial condition. As mentioned previously, Fokker-Planck equations of the general form given by Eq. (1) are employed to model the behavior of such systems. It is important to note that an analysis based on the FPE is one of many methods employed in the study of such systems and, for some cases, it may not be the appropriate description.<sup>28,29</sup>

In the present paper, three different problems with different choices  $A(x)$  and  $B(x)$  are chosen to demonstrate

the applicability of the discrete-ordinate method to the solution of Fokker-Planck equations of this type. The first is a model considered by Wehner and Wolfer,<sup>7</sup> defined by the following drift and diffusion coefficients:

$$A(x) = \frac{1}{4} \tanh(x) [1 - 2 \operatorname{sech}^2(x)], \quad (2a)$$

$$B(x) = \operatorname{sech}^2(x). \quad (2b)$$

An analytic solution of this FPE can be obtained with an appropriate change of variable as discussed in Sec. III A. The numerical solution will be compared with the exact solution and thus this study provides a useful check of the numerical methods employed.

The second FPE considered is one that has received considerable attention in the literature.<sup>30-32</sup> It is defined with the coefficients

$$A(x) = gx^3 - ax, \quad (3a)$$

$$B(x) = \epsilon. \quad (3b)$$

This FPE has been considered by many authors in a study of the role of fluctuations in systems far from equilibrium and the subsequent evolution of such systems. The main interest in this paper is to obtain numerical solutions for this system for a wide range of values of the parameters in Eq. (3). It is useful to note that in these studies,  $1/\epsilon$  is identified as the system size parameter and  $\epsilon$  is then a measure of the fluctuations in the system.<sup>4,28,30</sup> If  $\epsilon=0$ , a nonequilibrium state will relax deterministically to its equilibrium state, that is, if macroscopic variables initially have a fixed value, then at any subsequent time they will have fixed values. As  $\epsilon$  becomes larger, the fluctuations tend to dominate and the variance of the PDF  $P(x,t)$  becomes large.

Several workers have sought numerical and semianalytical solutions to Eq. (1) with  $A(x)$  and  $B(x)$  defined by Eq. (3). Among the methods used are scaling theory,<sup>33</sup> which is based on a nonlinear transformation of the FPE and is valid for  $\epsilon \rightarrow 0$ . Gaussian decoupling<sup>34</sup> is another method that applies in this limit and employs a Gaussian approximation of the solution at each time. Recently, Indira *et al.*<sup>30</sup> have employed a finite-element method and a Monte Carlo simulation to solve this FPE. They compared their essentially exact results with these approximate methods and suggest that the scaling theory is the most accurate method in the  $\epsilon \rightarrow 0$  limit.

The third example is an application to chemical reaction kinetics for a system with two stable states. The particular application is the *trans-gauche* isomerization of *n*-butane in carbon tetrachloride considered by Marechal and Moreau<sup>11</sup> and by Montgomery *et al.*<sup>12</sup> This system can be studied in an approximate fashion with the FPE and the coefficients

$$A(x) = \frac{1}{\nu m} \frac{dU(x)}{dx} \quad (4a)$$

and

$$B(x) = D, \quad (4b)$$

where  $\nu$  is the collision frequency,  $D$  is a diffusion coefficient, and  $U(x)$  is a double-well potential.

All these systems defined by the coefficients in Eqs. (2)–(4) have bimodal steady states. The method of solution of Eq. (1) employed in this paper is based on an eigenfunction expansion of  $P(x,t)$  as discussed by several authors.<sup>4,13,17-19,31,35</sup> The eigenfunctions and eigenvalues are determined with the numerical discrete-ordinate method (DO)<sup>36</sup> and associated nonclassical polynomials. The DO method of solution is based on the representation of the derivative operator  $d/dx$  and hence differential operators such as the operator defined by the right-hand side (rhs) of Eq. (1), in a discrete basis defined by a set of quadrature points. In a previous paper,<sup>36</sup> the method of representing the derivative and differential operators in a DO representation was discussed at length. A new quadrature procedure is introduced in this paper that reflects the bimodal nature of the equilibrium PDF that characterizes these bistable systems. The convergence of the eigenvalues and eigenfunctions is rapid with this method.

Although there exist other methods of solution, the eigenfunction expansion has the advantage of yielding eigenvalues which often have a useful physical interpretation. The reciprocal of the eigenvalues gives the fundamental relaxation times of the system and for these bistable systems the smallest finite eigenvalue can be related to the long-time rate coefficient<sup>10,13</sup> or the switching time in bimodal laser systems.<sup>15,16</sup> Also, for some systems, the FPE can be transformed to a Schrödinger equation<sup>4,35,37</sup> and the eigenvalues can be interpreted as the bound states in a potential derived from the coefficients in the FPE. The present results for the eigenvalues of the Fokker-Planck equations considered in this paper are superior to the results obtained to date by other workers. Many of these other calculations have been based on variational, WKB, and finite-element methods, and for the most part only a very restricted portion of the eigenvalue spectrum is obtained, and generally for a small range of the parameters in the coefficients. The DO method of solution of the FPE is outlined in Sec. II. Section III presents the results of the application of the DO method to several systems.

## II. SOLUTION OF THE FOKKER-PLANCK EQUATION

We begin our development with the standard eigenfunction expansion of  $P(x,t)$ .<sup>4,18,35</sup> In Sec. III B, we develop a technique to determine numerically these eigenfunctions and corresponding eigenvalues. In particular, Fokker-Planck (FP) equations with bimodal stationary solutions are considered, although the present method is by no means limited to such equations. We seek solutions to Eq. (1) which satisfy the boundary condition  $P(x,t) \rightarrow 0$  as  $x \rightarrow \pm \infty$ , for all of the models considered in this paper. Equation (1) may be rewritten as

$$\frac{\partial P(x,t)}{\partial t} = \tilde{L}P(x,t), \quad (5)$$

where  $\tilde{L}$  is the FP operator. The stationary solution of Eq. (1) is assumed to exist and is given by

$$P_0(x) = N \exp \left[ - \int_0^x \frac{A(x')}{B(x')} dx' - \ln[B(x)] \right], \quad (6)$$

where  $N$  is a normalization constant such that  $\int_{-\infty}^{\infty} P_0(x) dx = 1$ .  $P_0(x)$  plays an important role in the standard eigenfunction expansion since the eigenfunctions are orthonormal with respect to  $P_0^{-1}(x)$ . The formal solution of Eq. (5) is given by

$$P(x, t) = e^{\tilde{L}t} P(x, 0). \quad (7)$$

#### A. Eigenfunction expansion

The formal solution, Eq. (7), may be evaluated by expanding the initial distribution function in eigenfunctions of  $\tilde{L}$  and then applying  $e^{\tilde{L}t}$  term by term. Thus if  $P_n(x)$  are the eigenfunctions of  $\tilde{L}$ , defined by

$$\tilde{L}P_n(x) = -\lambda_n P_n(x), \quad (8)$$

we have the expansion

$$P(x, 0) = \sum_{n=0}^{\infty} a_n P_n(x), \quad (9)$$

where the expansion coefficients  $a_n$  are given by

$$a_n = \int_{-\infty}^{\infty} \phi_n(x) P(x, 0) dx. \quad (10)$$

The functions  $\phi_n$  in Eq. (10) are related to  $P_n$  by

$$\phi_n(x) = \frac{P_n(x)}{P_0(x)}, \quad (11)$$

and with Eqs. (8)–(11) we get from Eq. (7) the eigenfunction expansion

$$P(x, t) = \sum_{n=0}^{\infty} a_n \exp(-\lambda_n t) P_n(x). \quad (12)$$

Equation (12) is the standard eigenfunction expansion as discussed often in the literature. It is a useful description in that the reciprocals of the eigenvalues are the fundamental relaxation times of the system and the nature of the eigenvalue spectrum governs the approach of the system to equilibrium. It is useful to note that since  $\lambda_n > 0$ ,  $n > 0$ , and  $\lambda_0 = 0$ , then  $P(x, t) \rightarrow P_0(x)$  as  $t \rightarrow \infty$ .

The task, then, is to find the eigenfunctions and corresponding eigenvalues of Eq. (8). It is convenient to consider the transform of  $\tilde{L}$  of the form  $S^{-1}(x)\tilde{L}S(x)$  where  $S(x)$  is some positive-definite function. The eigenfunctions of the transformed operator are  $P_n(x)/S(x)$ . Two of these transformations have been widely used. The first is defined by  $S = P_0$ , giving the operator defined by

$$L = P_0^{-1} \tilde{L} P_0. \quad (13)$$

The eigenfunctions of  $L$ ,  $\phi_n(x)$ , are given by Eq. (11) and the eigenvalue equation  $L\phi_n = -\lambda_n \phi_n$  is given explicitly by

$$-A(x) \frac{d\phi_n(x)}{dx} + B(x) \frac{d^2\phi_n(x)}{dx^2} = -\lambda_n \phi_n(x), \quad (14)$$

where Eq. (13) has been used. With the definition Eq. (13), or the explicit form Eq. (14), it is clear that the operator  $L$  is self-adjoint with the scalar product defined with  $P_0(x)$  as the weight function. From a computational

standpoint, it is more convenient to consider Eq. (14) than Eq. (8) since  $\phi_n(x)$  are more slowly varying than  $P_n(x)$  and more easily evaluated [compare  $\phi_0 = 1$  and  $P_0(x)$ , Eq. (6)]. In addition, it is easier to obtain a symmetric representation of  $L$  than  $\tilde{L}$ , since in the former case a basis set orthonormal over  $P_0(x)$  is required while in the latter case a set of functions orthonormal over  $P_0^{-1}$  is needed, which is much more difficult to generate.

The second widely used transformation is defined by

$$\hat{L} = P_0^{-1/2} \tilde{L} P_0^{1/2}. \quad (15)$$

This form of the operator is self-adjoint with the scalar product defined with unit weight function. In particular, for systems for which  $B(x) = \epsilon$ , the eigenvalue problem may be cast into the form of a Schrödinger equation. The eigenfunctions  $\hat{\phi}_n$  satisfy

$$\epsilon \hat{\phi}_n''(x) - [V(x) - \lambda_n] \hat{\phi}_n(x) = 0, \quad (16)$$

where the potential  $V(x)$  is given by

$$V(x) = \frac{1}{2} \left[ \frac{[A(x)]^2}{2\epsilon} - \frac{dA(x)}{dx} \right]. \quad (17)$$

This is especially useful, since many techniques have been developed in quantum mechanics to find the eigenvalues and eigenfunctions of Eq. (16). Conversely, the techniques developed in this paper may be applied to problems of the form Eq. (16).

These are not the only transformations of the operator which are useful. In Sec. IIB it will be shown how to find a transformation  $S(x)$  for which a self-adjoint operator is defined with respect to an arbitrary weight function. With such a transformation, the DO method developed in Sec. IIIB becomes very flexible.

#### B. The discrete-ordinate method

The discrete-ordinate method, introduced by the authors in a previous paper,<sup>36</sup> is employed in the present paper to determine the eigenfunctions and eigenvalues of the Fokker-Planck operator. This method consists of representing functions, in particular the eigenfunctions and distribution functions, as column vectors  $\mathbf{f}$  whose  $N$  elements are  $f_i = w_i^{1/2} f(x_i)$ . The points  $\{x_i\}$  are the quadrature points, and  $\{w_i\}$  are the corresponding quadrature weights of some integration rule. This quadrature rule is defined by

$$\int_{-\infty}^{\infty} w(x) f(x) dx \simeq \sum_{i=0}^{N-1} w_i f(x_i), \quad (18)$$

where  $f(x)$  is some function defined on the interval  $(-\infty, \infty)$ , and  $w(x)$  is a suitable weight function. If  $f(x)$  is a polynomial of degree  $2N - 1$  or less, then Eq. (18) is exact.<sup>37</sup> The points  $\{x_i\}$  are the zeros of the  $N$ th-order polynomial,  $R_N(x)$ , of the set of polynomials orthonormal with respect to the weight function  $w(x)$ ; that is,

$$\int_{-\infty}^{\infty} w(x) R_n(x) R_m(x) dx = \delta_{nm}. \quad (19)$$

It was also shown,<sup>36</sup> provided that  $f(x)$  is a polynomial of degree less than  $N$ , that the representation of the function

$f(x)$  described above is equivalent to representing it as the vector of its expansion coefficients  $\underline{f}^p$  in the polynomial basis  $\{R_n(x)\}$ . The  $N$  components of  $\underline{f}^p$  are defined by

$$(\underline{f}^p)_n = \int_{-\infty}^{\infty} w(x)R_n(x)f(x)dx . \quad (20)$$

The equivalence of these representations is given by unitary transformation between the two bases, that is,

$$\underline{f} = \mathbf{T}^t \cdot \underline{f}^p , \quad (21)$$

where the elements of the matrix  $\mathbf{T}$  are

$$T_{nj} = R_n(x_j)w_j^{1/2} . \quad (22)$$

The basis of the DO method is the representation of the derivative operator  $d/dx$ , in the discrete space defined by the points in the quadrature rule, Eq. (18). This is easily done by using the transformation  $\mathbf{T}$  to transform the derivative operator from the polynomial basis to the DO basis, thus

$$D = \mathbf{T}^t \cdot \mathbf{D}^p \cdot \mathbf{T} , \quad (23)$$

where  $\mathbf{D}^p$  is the polynomial representation of the derivative operator and  $\mathbf{D}$  is the DO representation of this operator. The operator  $\mathbf{D}$  so constructed satisfies<sup>36</sup>

$$\underline{f}' = \mathbf{D} \cdot \underline{f} , \quad (24)$$

which represents a high-order algorithm for numerical differentiation based on quadrature weights and points. The matrix representative of differential operators can be written in a simple fashion by replacing derivatives with  $\mathbf{D}$ , and functions with their values at the set of points,  $\{x_i\}$ . Although one can proceed in this way with the solution of the eigenvalue problem, Eq. (14), it is useful to introduce a second set of functions, defined by

$$Q_n(x) = \left[ \frac{w(x)}{P_0(x)} \right]^{1/2} R_n(x) , \quad (25)$$

which are orthonormal with respect to  $P_0$ ; that is,

$$\int_{-\infty}^{\infty} P_0(x)Q_n(x)Q_m(x)dx = \delta_{nm} . \quad (26)$$

The matrix elements of the operator  $L$  in the basis  $\{Q_n(x)\}$  are given by

$$(\mathbf{L}^p)_{nm} = \int_{-\infty}^{\infty} P_0(x)Q_n(x)LQ_m(x)dx . \quad (27)$$

With an integration by parts, Eq. (27) becomes

$$(\mathbf{L}^p)_{nm} = - \int_{-\infty}^{\infty} P_0(x)B(x)Q_n'(x)Q_m'(x)dx . \quad (28)$$

It is clear that  $\mathbf{L}^p$  is symmetric in this representation and the superscript  $p$  denotes a representation in the polynomial basis  $\{R_n(x)\}$ . In terms of the polynomial set  $\{R_n(x)\}$  and the weight function  $w(x)$ , upon which the quadrature rule is based, we have, substituting Eq. (25) into Eq. (28), that

$$\begin{aligned} (\mathbf{L}^p)_{nm} &= - \int_{-\infty}^{\infty} B(x)w(x) \left[ \frac{d}{dx} + \frac{w'(x)}{2w(x)} - \frac{P_0'(x)}{2P_0(x)} \right] R_n(x) \\ &\quad \times \left[ \frac{d}{dx} + \frac{w'(x)}{2w(x)} - \frac{P_0'(x)}{2P_0(x)} \right] R_m(x)dx . \end{aligned} \quad (29)$$

It is important to note that Eq. (29) is not the representation of the operator  $L$  in the polynomial basis,  $\{R_n(x)\}$  defined by Eq. (13), which would be nonsymmetric, but rather it is the representation of the operator  $[P_0(x)w(x)]^{-1/2}\tilde{L}[P_0(x)w(x)]^{1/2}$ . This operator is symmetric in the polynomial basis  $\{R_n(x)\}$ . The relation Eq. (29) is a general relation independent of choice of basis and equilibrium weight, and has a form which is clearly appropriate for the quadrature rule, Eq. (18); thus,

$$\begin{aligned} (\mathbf{L}^p)_{nm} &\simeq - \sum_{k=0}^{N-1} B(x_k)w_k [R_m'(x_k) + g(x_k)R_m(x_k)] \\ &\quad \times [R_n'(x_k) + g(x_k)R_n(x_k)] , \end{aligned} \quad (30)$$

where

$$g(x) = \frac{w'(x)}{2w(x)} - \frac{P_0'(x)}{2P_0(x)} . \quad (31)$$

The derivative of  $R_n(x)$  may be evaluated with Eq. (24) and we have that

$$\begin{aligned} (\mathbf{L}^p)_{nm} &\simeq - \sum_{j=0}^{N-1} w_j^{1/2} R_m(x_j) \\ &\quad \times \sum_{i=0}^{N-1} w_i^{1/2} R_n(x_i) \\ &\quad \times \sum_{k=0}^{N-1} B(x_k) [D_{ki} + g(x_k)\delta_{ik}] \\ &\quad \times [D_{kj} + g(x_k)\delta_{jk}] , \end{aligned} \quad (32)$$

where the Kronecker  $\delta$  function has been introduced and the summations have been rearranged. The representation of the operator  $L$  in the DO basis may be written down by noting that the transformation between the two basis sets is given by

$$\mathbf{L} = \mathbf{T}^t \cdot \mathbf{L}^p \cdot \mathbf{T} . \quad (33)$$

With Eq. (32) and the unitarity condition,  $\mathbf{T}^t \cdot \mathbf{T} = \mathbf{I}$ , the unit matrix, we have that

$$L_{ij} \simeq - \sum_{k=0}^{N-1} B(x_k) [D_{ki} + g(x_k)\delta_{ik}] [D_{kj} + g(x_k)\delta_{jk}] . \quad (34)$$

The great advantage of the DO method is that the matrix representation of the FP operator is easily written down and evaluated for arbitrary coefficients  $A(x)$  and  $B(x)$ . Although any convenient set of polynomials,  $\{R_n(x)\}$ , could be employed, it is expected that the convergence of Eq. (12) would be rapid for  $w(x) = P_0(x)$ . For this case  $g(x) = 0$ , and  $L_{ij}$ , given by Eq. (34), is simplified. However, the polynomial basis set for this choice of weight function may be difficult to construct; hence alternate choices of basis sets need to be made, and Eq. (34) provides a symmetric DO representation for such basis sets.

### III. NUMERICAL APPLICATIONS

The numerical method developed in Sec. II will be applied to three FP equations discussed in Sec. I. Currently

there has been a great deal of interest in systems which have bistable steady states. Consequently, we have chosen to apply the DO method to this class of problems, although the DO method is applicable to a much wider class of problems. Since the equilibrium solutions are bimodal, it is desirable that the weight function  $w(x)$  also be bimodal.

There are no standard polynomial sets orthonormal over such weight functions, therefore we have generated sets of polynomials,  $\{R_n(x), n=0,1,\dots\}$ , orthonormal with respect to the weight functions defined by

$$w(\alpha,\gamma;x) = Ne^{-\gamma x^4/2 + \alpha x^2}, \quad (35)$$

where  $N$  is a normalization constant and  $\alpha$  and  $\gamma$  are two parameters. The weight function  $w(\alpha,\gamma;x)$  is the equilibrium distribution of the FP equation with the coefficients defined by Eq. (3) discussed at length in Sec. III B. The corresponding polynomials were generated specifically for the solution of this problem, although they are more widely applicable. This weight function is bimodal if both  $\alpha$  and  $\gamma$  are positive. The peaks are found at  $\pm(\alpha/\gamma)$  and the width of the peaks are inversely related to the size of  $\gamma$ . In the Appendix, we discuss the calculation of these polynomials, the calculation of the points and weights of the corresponding quadrature rule, and the construction of the derivative operator defined by Eq. (24). The three problems outlined in the introduction are solved with use of the sets of polynomials and corresponding weight functions described above.

#### A. Analytic example

In order to demonstrate the applicability of the present method, the FP equation defined by

$$\frac{\partial}{\partial t} P(x,t) = \frac{1}{4} \frac{\partial}{\partial x} \{ \tanh(x) [1 + 2 \operatorname{sech}^2(x)] P(x,t) \} + \frac{\partial^2}{\partial x^2} [ \operatorname{sech}^2(x) P(x,t) ] \quad (36)$$

is considered. This corresponds to the definitions of  $A(x)$  and  $B(x)$  given in Eq. (2). This equation was also considered by other authors.<sup>7,39</sup> The simple change of variable  $y = \frac{1}{2} \sinh(x)$  linearizes the drift coefficient of Eq. (36); thus, we find that

$$\frac{\partial P(y,t)}{\partial t} = \frac{1}{4} \left[ \frac{\partial y P(y,t)}{\partial y} + \frac{1}{2} \frac{\partial^2 (y,t)}{\partial y^2} \right]. \quad (37)$$

Equation (37) has the form of the standard "linear" FP equation and, with a  $\delta$ -function initial condition at  $y_0$ , has the solution<sup>2</sup>

$$P(y,t) = \frac{1}{[\pi(1-z^2)]^{1/2}} \exp \left[ -\frac{(y-zy_0)^2}{1-z^2} \right], \quad (38)$$

where  $z = e^{-t/4}$ . Substituting the definition of  $y$  into Eq. (38) and making use of  $dy = \frac{1}{2} \cosh(x) dx$  we have

$$P(x,t) = \frac{\cosh(x)}{[4\pi(1-z^2)]^{1/2}} \exp \left[ -\frac{[\sinh(x) - \sinh(x_0)z]^2}{4(1-z^2)} \right], \quad (39)$$

which is the desired result.

The first  $N$  eigenfunctions of the corresponding FP operator,  $L$ , of Eq. (37) may be determined exactly by using the method developed in Sec. II with  $N$  Hermite quadrature points and weights. This is a consequence of the fact that the adjoint of the operator on the rhs of Eq. (37) is precisely the Hermite differential operator divided by 8. The exact eigenvalues are

$$\lambda_n = n/4, \quad n=0,1,\dots \quad (40)$$

As a test of our method, the DO representation of the operator defined by Eq. (36), that is without the change of variable, was obtained with Eq. (34) in the DO basis, defined by the points and weights function  $w(2,2;x)$ . This matrix representation of the FP operator was diagonalized to give approximate eigenvalues and eigenfunctions. Table I shows the numerical convergence of  $4\lambda_n$  and as can be seen from the results in the table, 15 eigenvalues are converged to no less than four significant figures with 70 points.

The time-dependent PDF  $P(x,t)$  was determined for an initial  $\delta(x-x_0)$  distribution function with  $x_0 = -1.254$ , taken to coincide with one of the quadrature points. Although this gives an exact representation of the initial distribution function; it is clear that with a finite number of points the numerical solution will deviate from the exact result at sufficiently small times. However, the graph of the numerical  $P(x,t)$  shown in Fig. 1 for several times is indistinguishable from the analytic result. A total of 60 quadrature points were used in this calculation. Wehner and Wolfer<sup>7</sup> recently studied this model as a test of their numerical path-integral technique. Their method involves a propagation of the initial distribution in time, and the final calculated  $P_0(x)$  is within a few percent of the analytic result. Since the present method is based on an eigenfunction expansion and the lowest-order eigenfunc-

TABLE I. Convergence of eigenvalues. Example A.

$N$	$4\lambda_0$	$4\lambda_1$	$4\lambda_2$	$4\lambda_5$	$4\lambda_{10}$	$4\lambda_{15}$
10	0.0273	1.0277	2.941	8.998		
20	0.001 03	1.000 617	2.0900	5.679	23.3	51.86
30	0.000 010 4	1.000 003 76	2.003 11	5.0541	14.72	28.65
40	0.000 000 04	1.000 000 00	2.000 024 6	5.000 709	11.33	20.08
50	0.000 000 00	1.000 000 00	2.000 000 04	4.999 998 6	10.171	16.40
60	0.000 000 00	1.000 000 00	2.000 000 00	5.000 000 00	10.003 08	15.0934
70			2.000 000 00	5.000 000 00	10.000 003 44	14.996 59

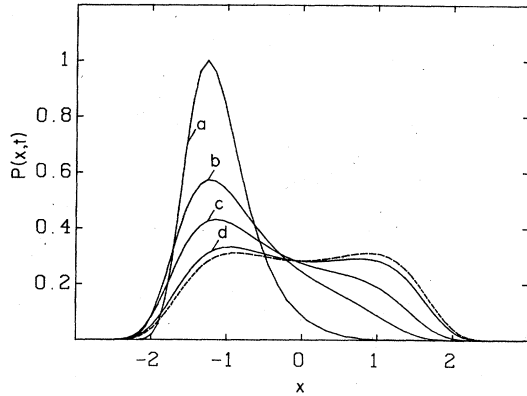


FIG. 1. Time variation of the probability density function for example A (see text);  $t$  is equal to, for curve a, 0.6; b, 2.0; c, 4.0; d, 10.0. — — — equilibrium distribution,  $P_0(x)$ .

tions are determined most accurately, the numerical result approaches more closely the true solution as  $t$  increases.

#### B. Diffusion in a bistable potential

A model FP equation that has received considerable attention recently is

$$\frac{\partial P(x,t)}{\partial t} = \frac{\partial[(gx^3 - ax)P(x,t)]}{\partial x} + \epsilon \frac{\partial^2 P(x,t)}{\partial x^2}. \quad (41)$$

Van Kampen<sup>2,4</sup> and Dekker and van Kampen,<sup>28</sup> have determined a few eigenvalues of this FPE. Suzuki<sup>5,33</sup> has employed this model in an application of scaling theory. A preliminary study, based on the DO method, was also carried out by the present authors<sup>8</sup> for the special case  $g=a=\epsilon=1$ . Recently Indira *et al.*<sup>30</sup> have obtained numerical solutions based on a finite-element method as well as with a Monte Carlo simulation. Brand *et al.*<sup>19</sup> have applied variational methods in the calculation of upper and lower bounds to the lowest two eigenvalues. The equilibrium solution is given by

$$P_0(x) = w(a/2\epsilon, g/2\epsilon; x), \quad (42)$$

and coincides with the weight function Eq. (35) with  $\alpha = a/2\epsilon$  and  $\gamma = g/2\epsilon$ . An immediate consequence of this is that the DO representation of the FP operator defined by Eq. (34) and the polynomial representation defined by Eq. (29) are equivalent. It is, however, more convenient to work in the polynomial basis since these matrix elements are simply related to the recurrence coefficients  $\beta_n$  that define the polynomials as discussed in the Appendix. If  $a$  and  $g$  are restricted to take on positive values, one can set  $a=g=1$  since all that is required is a redefinition of  $t$ ,  $x$ , and  $\epsilon$ . Thus the FP equation may be written as

$$\frac{\partial P(x,t)}{\partial t} = \frac{\partial[(x^3 - x)P(x,t)]}{\partial x} + \epsilon \frac{\partial^2 P(x,t)}{\partial x^2}, \quad (43)$$

where  $\epsilon$  is the only parameter and remains as a measure of either the system size or temperature.<sup>18</sup> The matrix elements of the operator  $L$ , Eq. (28),

$$L_{nm} = - \int_{-\infty}^{\infty} \epsilon w(1/2\epsilon, 1/2\epsilon; x) R_n'(x) R_m'(x) dx, \quad (44)$$

are given explicitly by

$$L_{nm} = \frac{\epsilon n^2}{\beta_n} + \frac{1}{\epsilon} \beta_n \beta_{n-1} \beta_{n-2}, \quad n=m \quad (45a)$$

$$L_{nm} = m(\beta_{m+2} \beta_{m+1})^{1/2}, \quad m=n-2 \quad (45b)$$

$$L_{nm} = n(\beta_{n+2} \beta_{n+1})^{1/2}, \quad n=m-2 \quad (45c)$$

$$L_{nm} = 0, \quad \text{otherwise} \quad (45d)$$

where the relation

$$R_n'(x) = \frac{n}{\beta_n^{1/2}} R_{n-1}(x) + \frac{1}{\epsilon} (\beta_n \beta_{n-1} \beta_{n-2})^{1/2} R_{n-3}(x), \quad (46)$$

derived in the Appendix, and the orthonormality of the polynomials have been used. The approximate eigenfunctions  $\phi_n(x)$  and eigenvalues, in the basis,  $\{R_n(x)\}$  are found by diagonalizing  $L$  given by Eq. (45). Since Eq. (45) defines a pentadiagonal matrix, the convergence of the eigenvalues and eigenfunctions is expected to be very rapid. If the differential operator on the right-hand side of this Eq. (43) is transformed to the Schrödinger form, Eq. (16), then the potential equation (17) is

$$V(x) = \frac{(x^3 - x)^2}{4\epsilon} - \frac{1}{2}(3x^2 - 1). \quad (47)$$

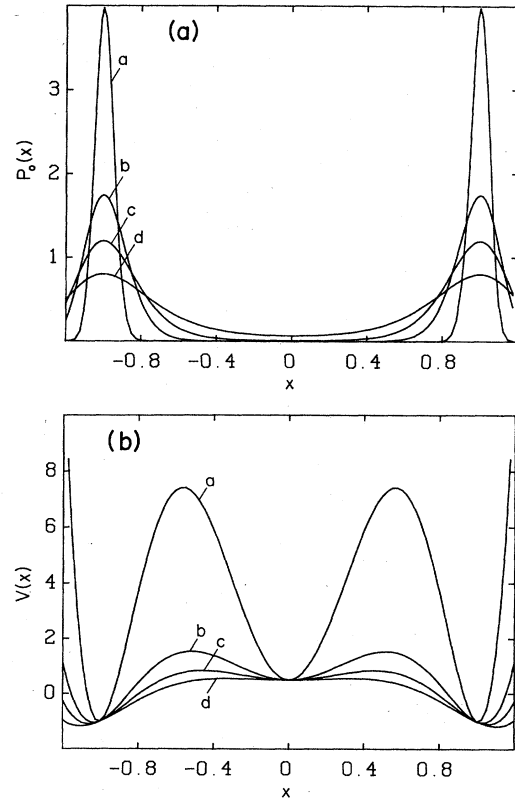


FIG. 2. (a) Potential in the Schrödinger equation, Eq. (47);  $\epsilon$  is equal to, for curve a, 0.005; b, 0.025; c, 0.05; d, 0.1. (b) Equilibrium distribution function, Eq. (42);  $\epsilon$  is equal to, for curve a, 0.005; b, 0.025; c, 0.05; d, 0.1.

TABLE II. Convergence of eigenvalues. Quartic potential ( $\epsilon=0.1$ ,  $a=g=1$ ). Numbers in parentheses signify powers of 10; i.e.,  $3.5016(-2)$  means  $3.5016 \times 10^{-2}$ .

$N$	$\lambda_1$	$\lambda_2$	$\lambda_3$	$\lambda_5$	$\lambda_{10}$	$\lambda_{15}$	$\lambda_{20}$	$\lambda_{25}$
3	1.15(-1)	1.64						
5	5.15(-2)	1.196	2.83					
8	3.5016(-2)	1.031	1.863	5.05				
10	3.3962(-2)	0.9647	1.7509	4.34				
15	3.3574302(-2)	0.928412	1.68828	3.8442	14.83			
20	3.3545699(-2)	0.927440	1.680430	3.738081	12.671	35.01		
30	3.3545300(-2)	0.927372	1.680264	3.733990	11.7001	23.299	43.33	74.83
40	3.3545300(-2)	0.927372	1.680264	3.733985	11.687463	22.64789	36.79	56.512
50				3.733985	11.687442	22.639923	36.04413	51.9850
60					11.687442	22.639908	36.031815	51.5419

The potential  $V(x)$ , and the corresponding equilibrium distribution  $P_0(x)$  are shown in Fig. 2 for various values of  $\epsilon$ . For sufficiently small values of  $\epsilon$ , this potential is characterized by the three minima at

$$x^0=0, \quad (48a)$$

$$x^\pm = \pm \left[ \frac{2}{3} + \left( \frac{1}{9} + 2\epsilon \right)^{1/2} \right]^{1/2}. \quad (48b)$$

The potential barriers between these three minima become larger as  $\epsilon$  becomes smaller. In the limit of  $\epsilon \rightarrow 0$ , approximate eigenvalues may be found by expanding the potential about the minima, keeping only the quadratic terms and neglecting terms of order  $\epsilon$ . The resulting harmonic potentials given by

$$V^\pm(x) = \frac{(x-x^\pm)^2}{\epsilon} - 1, \quad x \simeq x^\pm \quad (49a)$$

$$V^0(x) = \frac{x^2}{4\epsilon} + \frac{1}{2}, \quad x \simeq 0 \quad (49b)$$

approximate  $V(x)$  near  $x=x^\pm$  and  $x=x^0$ , respectively. The eigensolutions of Eq. (16) with the potentials defined by Eqs. (49) are given by

$$\hat{\phi}_k^\pm(x) = H_k((x-x^\pm)/\epsilon^{1/2}) \exp \left[ \frac{-(x-x^\pm)^2}{2\epsilon} \right], \quad (50a)$$

$$\hat{\phi}_k^0(x) = H_k(x/(2\epsilon)^{1/2}) \exp \left[ \frac{-x^2}{4\epsilon} \right], \quad (50b)$$

and their corresponding eigenvalues are given by

$$\lambda_k^\pm = 2k, \quad k=0,1,2,\dots \quad (51a)$$

$$\lambda_k^0 = k+1, \quad k=0,1,2,\dots \quad (51b)$$

where  $H_k$  is the  $k$ th Hermite polynomial. Thus in the limit of very small  $\epsilon$  the eigenvalues approach integer values. The zero eigenvalue is doubly degenerate and the remaining even eigenvalues are triply degenerate. In this limit, where there is no coupling between adjacent wells, the eigenfunctions  $\{\hat{\phi}_n(x)\}$  of Eq. (16) with  $V(x)$  given by Eq. (47) are linear combinations of  $\{\hat{\phi}_k^\pm(x), \hat{\phi}_k^0(x)\}$ . One such combination is given by

$$\hat{\phi}_n(x) = \frac{1}{\sqrt{2}} [\hat{\phi}_k^+(x) + \hat{\phi}_k^-(x)], \quad n=4k \quad (52a)$$

$$\hat{\phi}_n(x) = \frac{1}{\sqrt{2}} [\hat{\phi}_k^+(x) - \hat{\phi}_k^-(x)], \quad n=4k+1 \quad (52b)$$

$$\hat{\phi}_n(x) = \hat{\phi}_k^0(x), \quad n=2k+2, \quad k \text{ even} \quad (52c)$$

$$\hat{\phi}_n(x) = \hat{\phi}_k^0(x), \quad n=2k+1, \quad k \text{ odd} \quad (52d)$$

where the set  $\{\hat{\phi}_n(x)\}$  is obtained by letting  $k$  take on integer values in accordance with Eq. (52). This is not the only possible set of linear combinations that may be used, although it must be chosen such that  $\hat{\phi}_n$ 's come in even and odd pairs, since the potential given by Eq. (47) is even. This analysis is similar to the one given by Larson and Kostin<sup>13</sup> for a chemical kinetic model.

TABLE III. Convergence of eigenvalues. Quartic potentials ( $\epsilon=0.01$ ,  $a=g=1$ ).

$N$	$\lambda_1$	$\lambda_2$	$\lambda_3$	$\lambda_5$	$\lambda_{10}$	$\lambda_{15}$	$\lambda_{20}$	$\lambda_{25}$
10	3.37(-7)	1.866176	1.867351	3.52				
20	1.92(-10)	1.865756	1.865765	3.37	7.12	13.94		
30	1.05(-11)	1.865745	1.865754	3.307	5.23	9.41	17.53	29.37
40	6.452(-12)	1.150	1.865749	2.301	4.47	7.51	12.901	23.03
50	6.1681(-12)	0.9831	1.865725	1.9222	4.146	6.56	10.771	16.33
60	6.15498(-12)	0.96847	1.865337	1.86933	3.9797	6.114	9.543	14.18
70	6.1546497(-12)	0.967877	1.864581	1.867016	3.945756	5.9785	8.9845	12.986
80	6.1546497(-12)	0.967865	1.864542	1.866975	3.943588	5.96159	8.81464	12.433
90		0.967865	1.864542	1.866975	3.943532	5.960854	8.79404	12.284
100					3.943531	5.960839	8.793163	12.2693
DvK <sup>a</sup>		0.968	1.862	1.867				

<sup>a</sup>Dekker and van Kampen (see Ref. 28).

The numerical convergence of  $\lambda_n$  for  $\epsilon=0.1$  and  $0.01$  is given in Tables II and III, respectively. It is clear from the tables that the DO method is an efficient and accurate computational method for determining many excited states in this triple-well potential. The only other calculations of the eigenvalue spectrum include estimates of the lowest eigenvalues with variational methods,<sup>19</sup> estimates based on a finite difference calculation,<sup>28</sup> and asymptotic WKB approximations.<sup>31</sup> The smallest nonzero eigenvalue,  $\lambda_1$ , becomes very small as  $\epsilon$  decreases and as the barrier between adjacent wells [Fig. 2(a)] increases. It is interesting to note, especially for the smaller  $\epsilon$ , that some of the smaller eigenvalues converge more slowly than some larger eigenvalues; see  $\lambda_2$  and  $\lambda_3$  in Table III. The comparison of the rates of convergence in these two cases indicates the general trend that as  $\epsilon$  is decreased the rate of convergence of  $\lambda_n$  becomes slower. This may be understood in terms of the approximate eigenfunctions discussed above. The eigenfunctions are approximated by the square root of the equilibrium weight times a sum of the polynomials. When  $\epsilon$  is small some of the eigenfunctions are small in the region where the equilibrium weight is large and vice versa, consequently many basis functions are needed to represent those functions.

It is interesting to show the variation of the eigenvalues and eigenfunctions as a function of  $\epsilon$ . This is useful because it gives some indication of the validity of different approximation schemes. Figure 3 gives a plot of  $\log_{10}\lambda_1$  versus  $-\log_{10}\epsilon$ , which illustrates the very rapid decrease of this smallest nonzero eigenvalue with an increase in the barrier between the minima in the potential. The reciprocal of this eigenvalue corresponds to the relaxation time between the stable states. Figure 4 shows the variation of the eigenvalues  $\lambda_n$  ( $n=2-17$ ) for many of the excited states in this potential. The approach of the eigenvalue spectrum to the form in the  $\epsilon \rightarrow 0$  limit as given by Eq. (51) is clear from the figure. The asymptotic values of the eigenvalues to the right of the figure are very close to integer values, particularly for the lower states, and the successive singlet-triplet pattern is clearly seen. Figure 5 shows several of the eigenfunctions for  $\epsilon=0.01$ , which include some highly excited states. The features that are clear include the symmetric form of  $\hat{\phi}_n$  for  $n$  even and an-

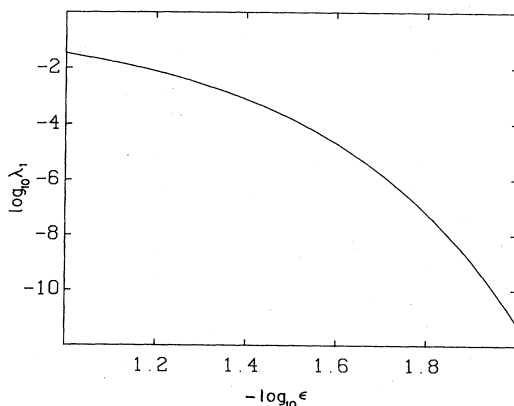


FIG. 3. Variation of  $\lambda_1$  with  $\epsilon$ ; Fokker-Planck operator defined by Eq. (43).

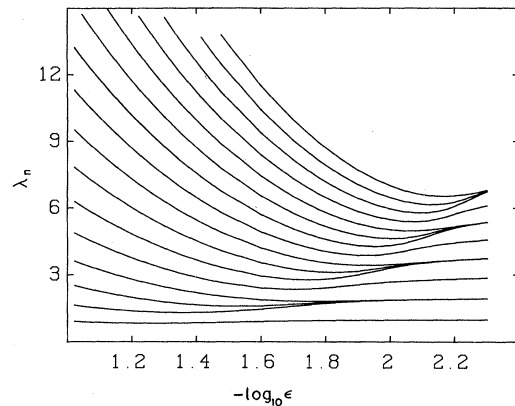


FIG. 4. Variation of  $\lambda_n$  with  $\epsilon$ ; Fokker-Planck operator defined by Eq. (43) with  $n=2$  (lowest curve) to  $n=17$ .

tisymmetric for  $n$  odd, and that the number of nodes is equal to  $n$ . It is interesting to note that  $\hat{\phi}_n$  for the lower states appear concentrated in the region of the minima of the potential  $V(x)$ . For the excited states ( $n=7$  and  $10$ ),  $\hat{\phi}_n$  is not concentrated near the minima. Figure 6 shows the variation of a particular eigenfunction  $\hat{\phi}_3(x)$  as a function of  $\epsilon$ . The eigenfunctions become more concentrated in the region of the minima of the potential with increasing  $\epsilon$ . It is interesting to note the dramatic change in the form of the eigenfunction between  $\epsilon = \frac{1}{140}$  and  $\frac{1}{180}$ . Figure 7 provides a comparison of the calculated  $\hat{\phi}_2(x)$  and the approximate form in terms of Hermite functions given by Eq. (52), valid for  $\epsilon \rightarrow 0$ . This comparison is useful since, together with Fig. 4, it suggests that the  $\epsilon \rightarrow 0$  limit is qualitatively attained for  $\epsilon \leq 0.01$ , at least for the lowest states.

The time-dependent solution of the FPE is completely determined once the expansion coefficients of the initial distribution are determined. For an initial  $\delta$ -function distribution  $\delta(x-x_0)$ , the PDF is given by

$$P(x,t) = \sum_{n=0}^{\infty} P_n(x) \phi_n(x_0) \exp(-\lambda_n t). \quad (53)$$

Figure 8 shows the time evolution of the distribution function for an initial  $\delta$ -function distribution with  $x_0=0$  and  $\epsilon=0.0125$ . The solid curves are the numerical results while the dashed curves are obtained with scaling theory,<sup>33</sup> valid in the limit  $\epsilon \rightarrow 0$ . As previously mentioned in Sec. III A, for an initial  $\delta$ -function distribution the numerical result with a finite number of polynomials will deviate from the actual solution for sufficiently small  $t$ . The numerical results shown in Fig. 8 employed 100 polynomials and are converged to the resolution of the graph except in the wings of the distribution at the smallest times; see Fig. 8(a),  $x \geq 0.6$ . The computation time for these calculations is less than the time reported by Indira *et al.*<sup>30</sup> with a finite-element method and considerably less than the time involved with the Monte Carlo simulations. However, one should note that the value of  $\epsilon$  used by these workers is very much less than we could use with existing algorithms.

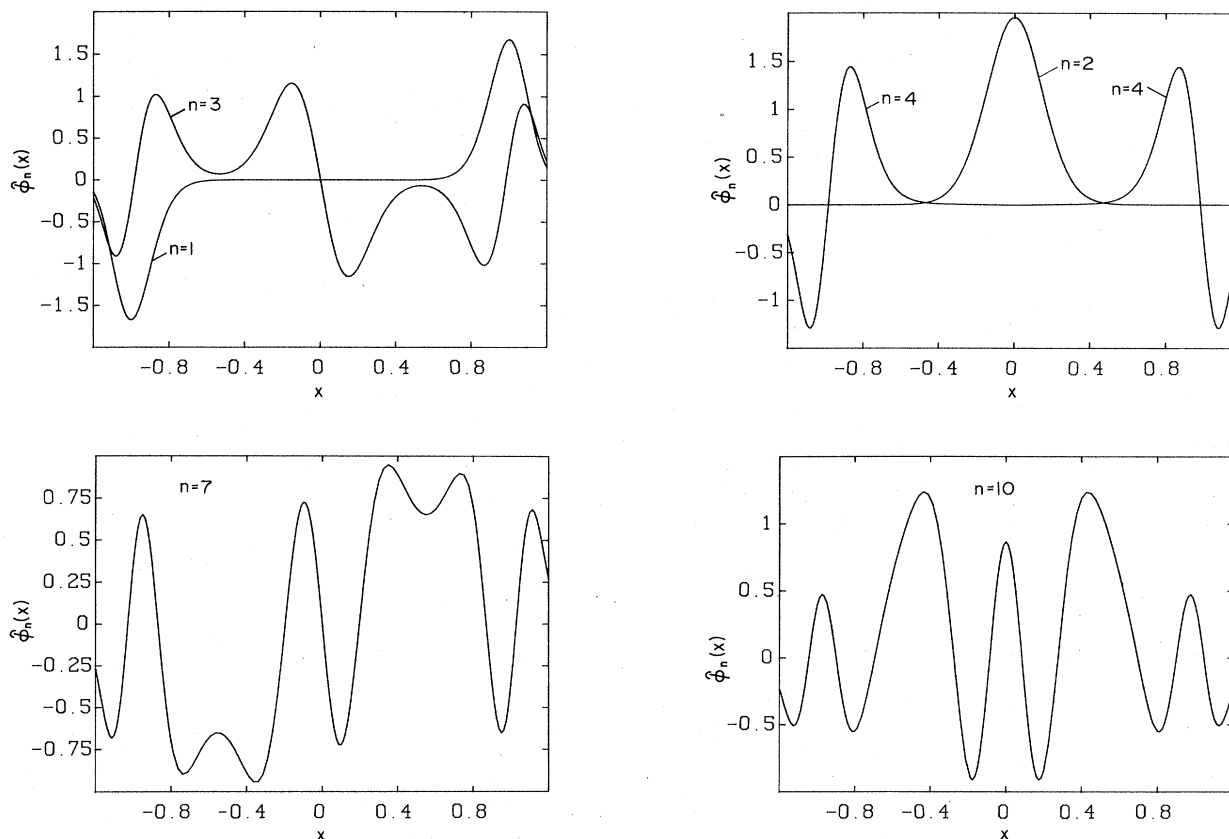


FIG. 5. Eigenfunctions  $\hat{\phi}_n(x)$ ; Eqs. (16) and (47).  $\epsilon=0.01$ .

From the results in Fig. 8, one can notice that the scaling-theory solution approximates the numerical calculations in some intermediate time regime as has been discussed by other authors.<sup>5,31,33</sup> The separation in the solid and dashed curves near  $x \approx 0$  Fig. 8(a) decreases with increasing  $t$ . However, the deviation of the scaling-theory result from the numerical solution increases for long times as shown in Fig. 8(b). There is some overlap in the two solutions at intermediate times. Caroli *et al.*<sup>31</sup> have shown that the normal mode expansion, Eq. (53), yields

Suzuki's scaling-theory result if the eigenvalues are approximated by their harmonic values, Eqs. (51), and the eigenfunctions are approximated by Weber functions. They then are able to approximately perform the sum in Eq. (53) and derive Suzuki's result. In terms of the present numerical results, it appears that Suzuki's result is valid at intermediate times for the following reasons. For small, but finite  $\epsilon$ , the largest eigenvalues will depart from the harmonic approximation and Suzuki's result will depart from the exact solution at short times, times for

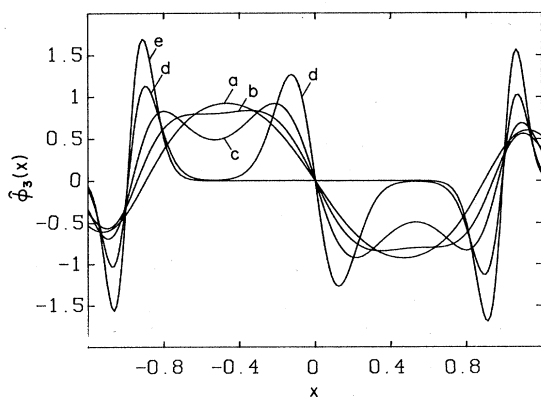


FIG. 6. Variation of  $\hat{\phi}_3$  with  $\epsilon$ ; Eqs. (16) and (47).  $\epsilon$  is equal to, for curve a,  $\frac{1}{20}$ ; b,  $\frac{1}{40}$ ; c,  $\frac{1}{60}$ ; d,  $\frac{1}{140}$ ; e  $\frac{1}{180}$ .

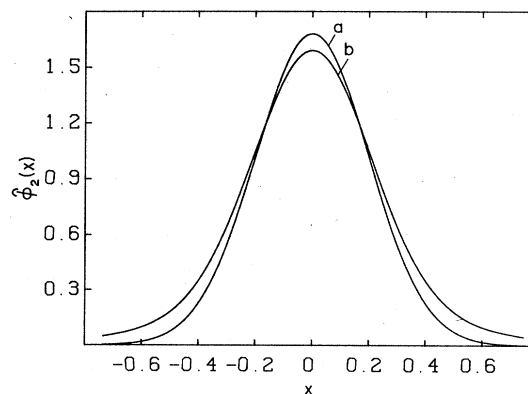


FIG. 7. Variation of  $\hat{\phi}_2(x)$ ; Eqs. (16) and (47).  $\epsilon=0.02$ . Curve a, harmonic approximation, see Eq. (52c); curve b, numerical result.

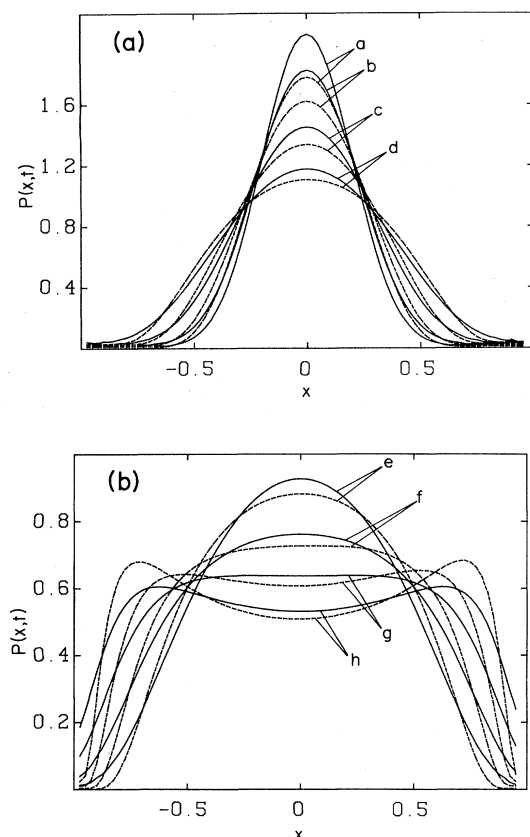


FIG. 8. Time variation of probability density function for  $\epsilon=0.0125$ . —, present result; ---, scaling-theory result.  $t$  is equal to, for curve  $a$ , 0.7;  $b$ , 0.8;  $c$ , 1.0;  $d$ , 1.2;  $e$ , 1.4;  $f$ , 1.6;  $g$ , 1.8;  $h$ , 2.0.

which the solution is dominated by the largest eigenvalues. With an increase in time the lower-order eigenvalues contribute most and if these are close to the harmonic values then Suzuki's solution will be close to the true solution. It should be noted, though, that scaling theory fails during a time regime for which the harmonic approximation of the eigenvalues is valid.

From the present study it appears that there are really only two rather than three distinct time domains as defined by  $1/\lambda_1$  and the reciprocal of some average eigenvalue  $1/\lambda_n$ ,  $n > 1$ . However, it is always possible to define different time regimes for which a group of eigenvalues makes a dominate contribution to the solution, but a comparable separation as occurs between  $\lambda_1$  and  $\lambda_2$  does not occur elsewhere in the spectrum.

### C. Chemical isomerization as a diffusion process

Chemical reactions can often be modeled as a diffusion process in configuration space in which reactants pass from a local potential minimum over a barrier to products.<sup>10-14</sup> The reactants and products represent two stable states of a bimodal potential and the reactive process is modeled with a FPE for a PDF in position as well as velocity. In the low-friction, or high-collision-rate, limit,<sup>12-14</sup> the approximate FPE is

$$\frac{\partial P(x,t)}{\partial t} = \frac{1}{\nu m} \frac{\partial [U'(x)P(x,t)]}{\partial x} + D \frac{\partial^2 P(x,t)}{\partial x^2}, \quad (54)$$

where  $\nu$  is the collision frequency,  $m$  is the reduced mass of the diffusing particle,  $D$  is the diffusion coefficient, and  $U(x)$  is the intramolecular potential. The equilibrium distribution is given by

$$P_0(x) = N e^{-U(x)/kT}, \quad (55)$$

where  $N$  is a normalization constant. The particular system studied corresponds to the *trans-gauche* isomerization of *n*-butane and has been considered recently by Marechal and Moreau<sup>11</sup> and Montgomery *et al.*<sup>12</sup> The potential employed in these studies is of the form

$$U(x) = \begin{cases} \frac{1}{2} m \omega_a^2 (x + x_a)^2, & x < -a \\ V_a - \frac{1}{2} m \omega_1^2 x^2, & -a < x < b \\ V_b + \frac{1}{2} m \omega_b^2 (x - x_b)^2, & x > b \end{cases} \quad (56)$$

where  $a = \hat{V}_a x_a$ ,  $b = \hat{V}_b x_b$ ,  $\omega_a^2 = \hat{V}_a \omega_1^2 / (1 - \hat{V}_a)$ , and  $\omega_b^2 = \hat{V}_b \omega_1^2 / (1 - \hat{V}_b)$  with  $\hat{V}_a = 2V_a / (m \omega_1^2 x_a)$  and  $\hat{V}_b = 2(V_a - V_b) / (m \omega_1^2 x_b)$ . The quantities  $a$ ,  $b$ ,  $\omega_a$ , and  $\omega_b$  are chosen such that the potential and first derivative are continuous. The other parameters used are given in Table IV and are chosen as in the previous papers.<sup>11,12</sup> With this potential the equilibrium distribution is bimodal.

The change in the concentration of isomers is given by a rate law of the form

$$\frac{d \delta N_A(t)}{dt} = -k(t) \delta N_A(t), \quad (57)$$

where

$$\delta N_A(t) = N_A^{\text{eq}} - N_A(t), \quad (58)$$

is the deviation from the equilibrium number of molecules in one conformation and  $k(t)$  is the time-dependent rate constant. An explicit expression for  $k(t)$  may be derived<sup>11</sup> assuming that the molecules have a Boltzmann distribution in one well and are absent from the other well. This expression is given by

$$k(t) = \sum_{n=0}^{\infty} A_n \exp(-\lambda_n t), \quad (59)$$

where

$$A_n = \lambda_n \left[ \int_0^{\infty} P_n(x) dx \right]^2. \quad (60)$$

TABLE IV. Potential parameters in *n*-butane isomerization.

$V_b = 2.93 \text{ kJ mole}^{-1}$
$V_a = 12.34 \text{ kJ mole}^{-1}$
$x_a = x_b = 1.57 \text{ \AA}$
$\omega_1 = 1.06 \times 10^{13} \text{ sec}^{-1}$
$\nu = 3.0 \times 10^{13} \text{ sec}^{-1}$
$T = 300 \text{ K}$
$m = 1.85 \times 10^{-23} \text{ g}$

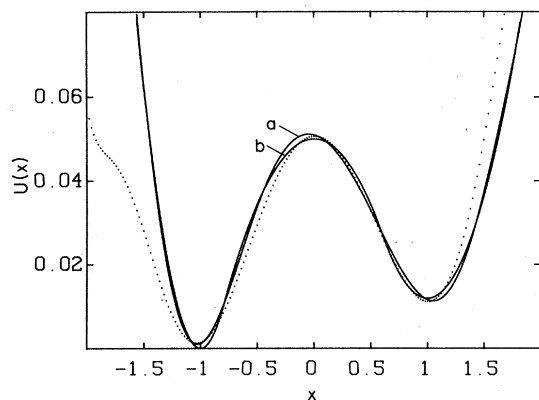


FIG. 9. Intramolecular potential for isomerization of *n*-butane.  $U(x)$  and  $x$  in units of  $m\nu^2x_a^2$  and  $x_a$ , respectively. —; curve *a*, harmonic potential Eq. (55); curve *b*, polynomial fit of harmonic potential. ···, polynomial fit of the true potential.

The time-dependent rate coefficient is then calculated with a knowledge of eigenfunctions  $P_n(x)$  and eigenvalues  $\lambda_n$  of the Fokker-Planck operator on the right-hand side of Eq. (54); that is,

$$\frac{1}{\nu m} \frac{d[U'(x)P_n(x,t)]}{dx} + D \frac{d^2P_n(x,t)}{dx^2} = -\lambda_n P_n(x,t). \quad (61)$$

In order to implement the present DO method, a fit of the potential was made with an 11th-order polynomial. In addition, a similar fit was made of the true potential<sup>40</sup> in

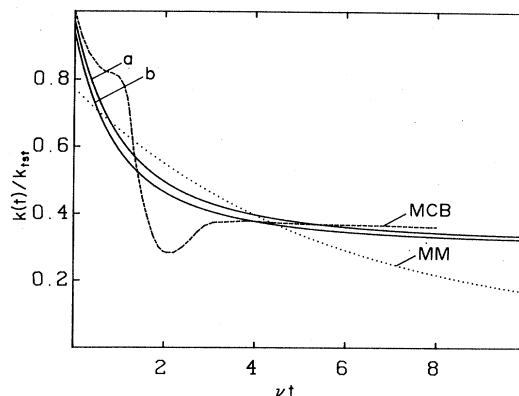


FIG. 10. Variation of the time-dependent coefficient. —; curve *a*, numerical fit of the harmonic potential; curve *b*, numerical fit of the true potential. ···, result of Marechal and Moreau (Ref. 11). ---, result of Montgomery, Chandler, and Berne (Ref. 12); the value of  $\nu$  used in Ref. 12 is listed as  $3 \times 10^{12} \text{ sec}^{-1}$ .

the region of interest. These three forms of the potential are given in Fig. 9. Approximate eigenvalues and eigenfunctions were obtained by diagonalizing the DO representation for this problem, Eq. (34), where  $P_0$  is given by Eq. (55) and the weight function is  $w(2,2;x)$ .

The expansion coefficients, Eq. (60), were evaluated approximately with the quadrature rule, Eq. (18),

$$A_n = \lambda_n \left[ \sum_{\substack{i=N/2 \\ N \text{ even}}}^{N-1} w_i P_n(x_i) \right]^2. \quad (62)$$

Table V shows the convergence of the eigenvalues versus

TABLE V. Convergence of eigenvalues: *n*-butane isomerization (harmonic potential).  $\lambda$  in units of  $3 \times 10^{13} \text{ sec}^{-1}$ .

$N$	$\lambda_1$	$\lambda_2$	$\lambda_3$	$\lambda_5$	$\lambda_9$
10	0.001 383 516	0.131 059 88	0.207 803 48	0.412 955 70	2.819 874 76
20	0.000 804 173	0.126 153 40	0.211 219 01	0.397 381 90	0.922 500 19
30	0.000 799 649	0.126 154 42	0.211 321 11	0.397 500 87	0.900 819 48
40	0.000 799 619	0.126 154 48	0.211 321 17	0.397 500 09	0.900 431 09
50	0.000 799 619	0.126 154 48	0.211 321 17	0.397 499 97	0.900 429 30
60				0.397 499 97	0.900 429 30

TABLE VI. Convergence of expansion coefficients for  $k(t)$  [harmonic potential, see Eq. (58)].  $A$  in units of  $3 \times 10^{13} \text{ sec}^{-1}$ .

$N$	$A_1$	$A_2$	$A_3$	$A_5$	$A_9$
10	2.814 97(−4)	0.437(−6)	7.863(−5)	2.026(−5)	5.304(−5)
20	1.814 66(−4)	2.348(−6)	3.737(−5)	2.117(−5)	5.485(−5)
30	1.782 71(−4)	1.999(−6)	3.490(−5)	1.963(−5)	3.818(−5)
40	1.782 33(−4)	1.900(−6)	3.409(−5)	1.879(−5)	3.385(−5)
50	1.782 22(−4)	1.856(−6)	3.369(−5)	1.837(−5)	3.159(−5)
60	1.782 16(−4)	1.831(−6)	3.346(−5)	1.814(−5)	3.035(−5)
70	1.782 12(−4)	1.815(−6)	3.332(−5)	1.799(−5)	2.960(−5)
80	1.782 09(−4)	1.804(−6)	3.322(−5)	1.789(−5)	2.910(−5)
90	1.782 07(−4)	1.797(−6)	3.315(−5)	1.782(−5)	2.875(−5)

TABLE VII. Comparison of transition times for *n*-butane isomerization.  $\tau$  in units of  $10^{-11}$  sec,  $A$  in units of  $10^9$  sec $^{-1}$ .

<i>n</i>	Marechal and Moreau <sup>a</sup>		Fitted harmonic		Fitted actual	
	$\tau_n$	$A_n$	$\tau_n$	$A_n$	$\tau_n$	$A_n$
1	3.7	0.743	4.17	5.35	3.86	5.20
2	0.027	1.95	0.0264	0.0539	0.0249	0.0338
3	0.017	10.0	0.0157	0.994	0.0204	0.112
4			0.0110	1.06	0.0149	0.975
5			0.0084	0.0535	0.0114	0.0093
6			0.0066	1.54	0.0085	1.64

<sup>a</sup>Reference 11.

the number of quadrature points. As can clearly be seen from the table, the rate of convergence of the eigenvalues is extremely rapid in contrast to the suggestion of previous workers.<sup>12</sup> As expected,  $\lambda_1$  is well separated from the other eigenvalues and corresponds to the rate of diffusion from one state to the other. The rate of convergence of the expansion coefficients  $A_n$  in the expression for  $k(t)$ , Eq. (59), is shown in Table VI. These converge more slowly than the eigenvalues primarily due to our use of the quadrature rule designed for the range  $(-\infty, \infty)$  for the integration in Eq. (60) which is on the range  $(0, \infty)$ . Since we are interested in the long-time behavior of  $k(t)$  for which only the lower-order  $A_n$  coefficients contribute, the present results are satisfactory. Also, it is important to note that  $A_1 > A_2$  which, together with  $\lambda_1 \ll \lambda_2$ , assures a limiting rate law. The present results for the two different fits of the potential are compared together with the limited results of Marechal *et al.* in Table VII. This table shows that the present values of the relaxation times  $\tau_n = 1/\lambda_n$  agree to within 10% of those by Marechal and Moreau while the  $A_n$  differ by factors of the order of 10.

Figure 10 shows a graph of the ratio  $k(t)/k_{\text{tst}}$  versus  $vt$ , where  $k_{\text{tst}}$  is the rate obtained from transition-state theory. The results obtained by Montgomery *et al.* and Marechal and Moreau are also shown. The result of Marechal and Moreau does not agree with the present result nor with that of Montgomery *et al.* Their result for  $A_1$ , which is the value of  $k(t)$  as it approaches a constant value, is too low. This is probably due to the WKB approximation used, which is not valid in regions where two classical turning points are near each other, which is the case for the present model. An indication of the extent to which the eigenfunction expansion, Eq. (59), converges is given by how close to unity is  $k(0)/k_{\text{tst}}$ . Although up to 90 quadrature points are used for the calculation of  $\lambda_n$  for the results in Fig. 10, only 14 and 18 terms were retained for curves *a* and *b*, respectively. The restriction to this small number of terms is due to the way which the  $A_n$  were calculated with Eq. (62), as discussed previously. It may be noted that with the present treatment it is impossible to obtain the structure in  $k(t)$  found by Montgomery *et al.*<sup>12</sup> since the present  $k(t)$  must be a monotonic decreasing function as all the  $A_n$  are positive. However, the present result for the plateau value of  $k(t)/k_{\text{tst}}$  is in very good agreement with Montgomery *et al.*<sup>12</sup> The asymptotic value for  $k(t)/k_{\text{tst}}$  obtained by Marechal and Moreau of 0.045 is much too low.

#### IV. SUMMARY

The present paper has demonstrated the application of the discrete-ordinate method to the solution of a large class of Fokker-Planck equations. The method is computationally accurate and efficient for a wide variety of coefficients in the Fokker-Planck equation. The great advantage of the present discrete-ordinate method lies in the ease with which the symmetric-matrix representation of the differential operator may be generated, and the flexibility with respect to the choice of basis functions and quadrature points. Since some Fokker-Planck equations considered are equivalent to a Schrödinger equation, the present method is also applicable to quantum-mechanical problems.

In the application of the discrete-ordinate method to three Fokker-Planck equations, we have demonstrated the very rapid convergence of the eigenvalues of the Fokker-Planck operator with different diffusion and drift coefficients. The time evolution of the probability density function has been easily determined, and the bifurcations which occur in these bistable systems were studied. Work is in progress toward an extension of the discrete-ordinate method to other basis sets and to two-dimensional problems.

#### ACKNOWLEDGMENTS

This research is supported by a grant from the Natural Sciences and Engineering Research Council of Canada.

#### APPENDIX: POLYNOMIAL BASIS AND DERIVATIVE OPERATOR

In this appendix we develop a recurrence relation for the recurrence coefficients for a set of polynomials which are orthonormal over the bimodal weight function given by Eq. (35). The corresponding quadrature weights and points, and the derivative operator in the DO basis, are also calculated. The set of polynomials are defined such that  $R_n(x)$  is a polynomial of degree  $n$ . These polynomials may be generated from a three-term recurrence relation of the form

$$\beta_{n+1}^{1/2} R_{n+1}(x) = (x - \alpha_n) R_n(x) - \beta_{n-1}^{1/2} R_{n-1}(x). \quad (\text{A1})$$

The  $\alpha_n$  are related to odd moments of  $w(x)$  by

$$\alpha_n = \int_{-\infty}^{\infty} w(\alpha, \gamma; x) [R_n(x)]^2 x dx . \tag{A2}$$

The relation Eq. (A2) was derived by multiplying Eq. (A1) by  $w(x)R_n(x)$  and integrating. The  $\alpha_n$  must all vanish since the weight function is an even function and hence we are left with the simpler recurrence relation,

$$\beta_{n+1}^{1/2} R_{n+1}(x) = x R_n(x) - \beta_{n-1}^{1/2} R_{n-1}(x) . \tag{A3}$$

The  $\beta_n$  were generated by a method similar to one previously employed,<sup>40</sup> based on the Cristoffel-Darboux identity,

$$\sum_{k=0}^n [R_k(x)]^2 = \beta_{n+1}^{1/2} [R_n(x)R'_{n+1}(x) - R_{n+1}(x)R'_n(x)] . \tag{A4}$$

When Eq. (A4) is multiplied by  $w(\alpha, \gamma; x)$  and integrated we obtain

$$n + 1 = \beta_{n+1}^{1/2} \int_{-\infty}^{\infty} w(\alpha, \gamma; x) R_n(x) R'_{n+1}(x) dx , \tag{A5}$$

where the second integral vanishes since  $R'_n(x)$  is orthogonal to  $R_n(x)$ . The rhs of Eq. (A5) may be integrated by parts, yielding

$$n + 1 = \beta_{n+1}^{1/2} \int_{-\infty}^{\infty} (\gamma x^3 - \alpha x) w(\alpha, \gamma; x) R_n(x) R_{n+1}(x) dx . \tag{A6}$$

Finally, with the repeated application of Eq. (A3), the integral in Eq. (A6) may be evaluated giving, with some rearrangement,

$$\beta_{n+2} = \frac{n+1}{\gamma \beta_{n+1}} + \frac{\alpha}{\gamma} - \beta_{n+1} - \beta_n . \tag{A7}$$

---


$$I(m) = 2 \left[ \frac{2}{\gamma} \right]^{(m+1)/4} \left[ \Gamma\left(\frac{1}{4}(m+1)\right) + \alpha \left[ \frac{2}{\gamma} \right]^{1/2} \Gamma\left(\frac{1}{4}(m+3)\right) \right. \\ \left. + \Gamma\left(\frac{1}{4}(m+1)\right) \sum_{n=1}^{\infty} \frac{1}{2n!} \left[ \frac{2\alpha^2}{\gamma} \right]^n \left[ \prod_{k=1}^n \left[ k + \frac{1}{4}(m-3) \right] \right] \right. \\ \left. + \alpha \left[ \frac{2}{\gamma} \right]^{1/2} \Gamma\left(\frac{1}{4}(m+3)\right) \sum_{n=1}^{\infty} \frac{1}{(2n+1)!} \left[ \frac{2\alpha^2}{\gamma} \right]^n \left[ \prod_{k=1}^n \left[ k + \frac{1}{4}(m-1) \right] \right] \right] . \tag{A11}$$

By including enough terms in this expansion the first two moments could be evaluated to any degree of accuracy. The gamma function was evaluated by breaking it up into two pieces,

$$\Gamma(a) = \int_0^x y^{a-1} e^{-y} dy + \gamma(a, x) . \tag{A12}$$

The first integral of Eq. (A12) was evaluated by expanding the integrand and integrating term by term. The incomplete gamma function has a continued-fraction expansion,<sup>41</sup>

Equation (A7) is the desired result. All the  $\beta_n$  may be found by recurrence if  $\beta_1$  is known, since  $\beta_0$  is equal to 0. It may be determined by setting  $n=0$  in Eq. (A3) and squaring and integrating. This gives, with some rearrangement,

$$\beta_1 = \int_{-\infty}^{\infty} w(\alpha, \gamma; x) x^2 dx , \tag{A8a}$$

$$= \frac{\int_{-\infty}^{\infty} e^{-\gamma x^4/2 + \alpha x^2} x^2 dx}{\int_{-\infty}^{\infty} e^{-\gamma x^4/2 + \alpha x^2} dx} . \tag{A8b}$$

As in the previous paper,<sup>40</sup> the recurrence relation, Eq. (A7), for the recurrence coefficients suffers from round-off error and it is therefore necessary to use high precision when the  $\beta_n$  are calculated. Thus the two integrals

$$I(m) = \int_{-\infty}^{\infty} x^m e^{-\gamma x^4/2 + \alpha x^2} dx, \quad m=0 \text{ and } 2 \tag{A9}$$

must be evaluated essentially exactly.

These integrals were evaluated in the following manner. The  $\exp(\alpha x^2)$  factor in the integrand was expanded in a Taylor-series expansion and the resulting integrals were evaluated term by term, yielding

$$I(m) = 2 \left[ \frac{2}{\gamma} \right]^{(m+1)/4} \sum_{n=0}^{\infty} \frac{1}{n!} \left[ \frac{2\alpha^2}{\gamma} \right]^{n/2} \Gamma\left(\frac{1}{4}(m+2n+1)\right) . \tag{A10}$$

With Eq. (A10) written out term by term and the use of the recurrence relation for the gamma function, we have that

---


$$\gamma(a, x) = \frac{e^{-x} x^a}{x + \frac{1-a}{1 + \frac{1}{x + \frac{2-a}{1 + \frac{2}{x + \dots}}}}} . \tag{A13}$$

With the use of Eqs. (A11)–(A13) the integrals in Eq. (A9) were evaluated to 115 decimal places and the  $\beta_n$  were then evaluated with the use of Eq. (A7).

We now wish to develop a discrete-ordinate derivative operator as described previously. To do this we first find

the matrix representation of the derivative operator in the polynomial basis; that is,

$$(\mathbf{D}^p)_{nm} = \int_{-\infty}^{\infty} w(\alpha, \gamma; x) R_n(x) R_m'(x) dx. \quad (\text{A14})$$

From Eq. (A5) it follows directly that

$$(\mathbf{D}^p)_{nm} = (n+1)\beta_{n+1}^{-1/2}, \quad m = n+1. \quad (\text{A15})$$

The other matrix elements may be evaluated by integrating Eq. (A14) by parts. With repeated use of the recurrence relation, Eq. (A3), it may be shown that the only other nonzero matrix elements are those for which  $m = n+3$ . Thus we have that

$$(\mathbf{D}^p)_{nm} = 2\gamma(\beta_{n+1}\beta_{n+2}\beta_{n+3})^{1/2}, \quad m = n+3 \quad (\text{A16})$$

and

$$(\mathbf{D}^p)_{nm} = 0, \quad \text{otherwise (i.e., } m \neq n+2 \pm 1). \quad (\text{A17})$$

Equations (A15)–(A17) define the polynomial representation of the derivative operator. The corresponding DO representation may be found with Eq. (23). The quadrature points and weights were found by diagonalizing the symmetric tridiagonal Jacobi matrix defined by

$$X_{nm} = \beta_n, \quad n = m+1 \quad (\text{A18a})$$

$$X_{nm} = \beta_m, \quad m = n+1 \quad (\text{A18b})$$

$$X_{nm} = 0, \quad \text{otherwise (i.e., } |n-m| \neq 1). \quad (\text{A18c})$$

where the quadrature points are the eigenvalues of this matrix and the weights are the square of the first element of the eigenvectors.<sup>37</sup>

- <sup>1</sup>H. Haken, *Rev. Mod. Phys.* **47**, 67 (1975).  
<sup>2</sup>N. G. van Kampen, *Stochastic Processes in Chemistry and Physics* (North-Holland, Amsterdam, 1981); H. Risken, *The Fokker-Planck Equation* (Springer, New York, 1984).  
<sup>3</sup>H. Haken, *Synergetics*, 2nd ed. (Springer, Berlin, 1979).  
<sup>4</sup>N. G. van Kampen, *J. Stat. Phys.* **17**, 71 (1977).  
<sup>5</sup>M. Suzuki, *Adv. Chem. Phys.* **46**, 195 (1981).  
<sup>6</sup>S. Chandrasekhar, *Rev. Mod. Phys.* **15**, 1 (1943).  
<sup>7</sup>M. Wehner and W. G. Wolfer, *Phys. Rev. A* **27**, 2663 (1983); **28**, 3003 (1983).  
<sup>8</sup>B. Shizgal and R. Blackmore, *Chem. Phys. Lett.* **109**, 242 (1984).  
<sup>9</sup>P. S. Hubbard, *Phys. Rev. A* **19**, 907 (1979).  
<sup>10</sup>H. A. Kramers, *Physica* **7**, 284 (1940).  
<sup>11</sup>E. Marechal and M. Moreau, *Mol. Phys.* **51**, 133 (1984).  
<sup>12</sup>J. A. Montgomery, Jr., D. Chandler, and B. Berne, *J. Chem. Phys.* **70**, 4056 (1979).  
<sup>13</sup>R. S. Larson and M. Kostin, *J. Chem. Phys.* **69**, 4821 (1978); **72**, 1392 (1980).  
<sup>14</sup>J. L. Skinner and P. G. Wolynes, *J. Chem. Phys.* **69**, 2143 (1978); B. Carmeli and A. Nitzan, *ibid.* **80**, 3596 (1984).  
<sup>15</sup>C. M. Bowden, M. Ciften, and H. R. Roble, *Optical Bistability* (Plenum, New York, 1981).  
<sup>16</sup>R. Bonifacio, *Dissipative Systems in Quantum Optics* (Springer, Berlin, 1982).  
<sup>17</sup>R. Graham and A. Schenzle, *Phys. Rev. A* **23**, 1302 (1981).  
<sup>18</sup>A. Schenzle and H. Brand, *Phys. Rev. A* **20**, 1628 (1979).  
<sup>19</sup>H. Brand, A. Schenzle, and G. Schroder, *Phys. Rev. A* **25**, 2324 (1982).  
<sup>20</sup>K. Andersen and K. E. Shuler, *J. Chem. Phys.* **40**, 633 (1964).  
<sup>21</sup>M. R. Hoare, *Adv. Chem. Phys.* **20**, 135 (1971).  
<sup>22</sup>B. Shizgal, *J. Chem. Phys.* **70**, 1948 (1979).  
<sup>23</sup>B. Shizgal, *Chem. Phys. Lett.* **100**, 41 (1983).  
<sup>24</sup>R. I. Cukier, K. L. Lindenberg, and K. E. Shuler, *J. Stat. Phys.* **9**, 137 (1973).  
<sup>25</sup>M. O. Hongler and W. M. Zheng, *J. Stat. Phys.* **29**, 317 (1982); W. M. Zheng, *J. Math. Phys.* **25**, 88 (1984).  
<sup>26</sup>M. O. Hongler and R. C. Desai, *J. Stat. Phys.* **32**, 585 (1983).  
<sup>27</sup>M. C. Valsakumar, *J. Stat. Phys.* **32**, 545 (1983).  
<sup>28</sup>H. Dekker and N. G. van Kampen, *Phys. Lett.* **73A**, 374 (1979).  
<sup>29</sup>P. Hänggi, H. Grabert, P. Talkner, and H. Thomas, *Phys. Rev. A* **29**, 371 (1981).  
<sup>30</sup>R. Indira, M. C. Valsakumar, K. P. N. Murthy, and G. Ananthakrishna, *J. Stat. Phys.* **33**, 181 (1983).  
<sup>31</sup>B. Caroli, C. Caroli, and B. Roulet, *J. Stat. Phys.* **21**, 415 (1979).  
<sup>32</sup>B. Caroli, C. Caroli, and B. Roulet, *J. Stat. Phys.* **26**, 83 (1981).  
<sup>33</sup>M. Suzuki, *Order and Fluctuations in Equilibrium and Non-equilibrium Statistical Mechanics* (Wiley, New York, 1981).  
<sup>34</sup>A. Budgor, *J. Stat. Phys.* **15**, 375 (1976).  
<sup>35</sup>H. Tomita, A. Ito, and H. Kidachi, *Prog. Theor. Phys.* **56**, 786 (1976).  
<sup>36</sup>B. Shizgal and R. Blackmore, *J. Comput. Phys.* **55**, 313 (1984).  
<sup>37</sup>P. Davis and P. Rabinowitz, *Methods of Numerical Integration* (Academic, New York, 1975).  
<sup>38</sup>J. C. Zambrini and K. Yasue, *Ann. Phys. (N.Y.)* **125**, 176 (1980).  
<sup>39</sup>B. Shizgal, *J. Comput. Phys.* **41**, 309 (1981).  
<sup>40</sup>R. Scott and H. Scheraga, *J. Chem. Phys.* **44**, 3054 (1966).  
<sup>41</sup>M. Abramowitz and I. A. Stegun, *Handbook of Mathematical Functions* (Dover, New York, 1964).